THE JOURNAL OF PHYSICAL CHEMISTRY A

ARTICLE

pubs.acs.org/JPCA

Modeling Chemical Evolution in a Cold Molecular Plasma: Quantum Dynamics of CF_2^- Intermediates after Electron Attachment

F. Sebastianelli, F. Carelli, and F. A. Gianturco*

Department of Chemistry and CISM, The University of Rome "Sapienza", P.le Aldo Moro 5, 00185 Rome, Italy

ABSTRACT: A dynamical study is presented for the chemical processes induced by electrons (with energies up to about 16 eV) on gaseous CF_2 (X^1A_1 state), one of the important components of plasma etching molecular mixtures. The nuclear deformations from the C_{2v} initial geometry are seen to lead to different anionic intermediates that suggest different chemical evolutions into final fragments. All nuclear motions are shown to be effective for the formation of a variety of resonances which could lead to different final fragments. The effect of the above vibrational activation of the transient anionic states initially formed at the equilibrium geometry is analyzed and discussed in detail, providing compelling evidence and physical reasons for the fragment observations given by various experiments on such plasmas.

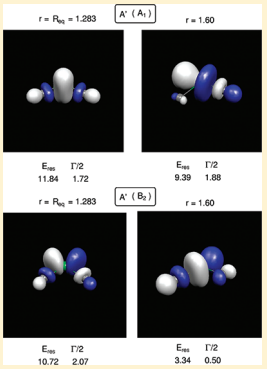

I. INTRODUCTION

The possibility of selectively etching silicon wafers using molecular plasmas has been one of the chief causes for the many advances in the industry of computer components. The general procedure for forming such plasmas involves the bombarding with electrons of a set of so-called "feedstock gases", in order to produce chemically active molecular radicals or fragment ions. Unfortunately, rather little is still known about the molecular features of the processes involved or of the chief characteristics which allow for an efficient evolution of the etching processes.[1] One therefore needs to put together as many as possible models which can provide us with an interpretation, at the molecular level, of the important steps undergone by the molecules of the feedstock gases after the initial electron impact to neutral gas. Recent topical issues in the current literature[2,3] have highlighted the need to provide a firmer grounding of the technological applications with nanoscopic models of the physics involved that are as detailed as possible: hence the motivation for the present study.

Fluorine-containing molecules, i.e., the large family of fluorocarbons, have been selected in many cases as one of the most interesting families of feedstock gases since they are considered to be efficient mediators for the production of highly reactive intermediates after the electron-impact activation, together with the production of radical species.[4−6] As a consequence of such properties, theoretical and experimental interest in CF_x and SiF_x (x = 1, 2, 3, and 4) compounds, and in their properties when interacting with electron probes, has grown quite markedly since any knowledge of the various cross sections describing the numerous possible outcomes constitutes an important step in determining the ensuing plasma properties, thereby becoming important tools for plasma modeling studies. In particular, the smaller CF_x species are of great interest because they are thought to be responsible for the actual etching of the underlying wafers when the used feedstock gases are carbon perfluoride compounds, with general formulas C_nF_{2n+2}. Such precursor molecules, in fact, fragment into various CF_x radicals when bombarded by electrons, but little is actually known about the features of such nascent radicals and about their specific evolution when further interacting with the plasma's ambient electrons.[7]

In the present study we specifically intend to analyze, from a theoretical and computational standpoint, the behavior of an apparently simple fluorocarbon radical, the CF_2 molecule, once it is made to interact with low-energy electrons. We shall follow its evolution along possible fragmentation pathways related to the formation of temporary negative ions (TNIs) by resonant electron attachment processes. There have been several studies, in fact, which have dealt with this radical species: for example, the ionizing cross sections were reported in ref 7 and electron-impact-ionization cross sections were calculated in ref 8 using a semiclassical modeling, with the latter turning out to be larger than the measured data. More recent calculations for the same ionization cross sections[9] also produced results about 5% higher than experiments. Elastic differential cross sections for the CF_x (x = 1, 2, 3) radicals have been reported in ref 10. Very few data, however, exist in the low-energy range (e.g., around and below 15 eV) of electron collision processes with this radical. R-matrix calculations of $e^-−CF_2$ at its equilibrium geometry, and for energies below 10 eV, have been published recently.[11] The calculations presented three groups of excitation cross sections: of the $^3B_1$ state, of the bound $^1B_1$ state, and of the sum of the remaining three dissociative states $^3A_2$, $^1A_2$, and $^3B_2$. They also found a $^2B_1$ shape resonance around 1 eV, suggesting that a small

Received: July 12, 2011
Revised: September 13, 2011
Published: September 13, 2011

part of it may dissociate into $CF(^2\Pi) + F^-(^1S)$, while the largest part decays into a vibrationally excited $(CF_2^-)^*$ stable molecule. Another resonance, considered to be a shape resonance, was found as a $^2A_1$ metastable state around 6 eV that drives the $^2A_1 \rightarrow {}^3B_1$ excitation process.[11] Further theoretical results were presented in ref 12 at low and intermediate energies, showing angular distributions calculated using a complex optical potential within the iterative Schwinger variational method and combined with the distorted-wave approximation. Their low-energy integral elastic cross sections locate again a $^2B_1$ shape resonance around 1.5 eV but with different details from those in ref 11. They also found another resonance of $^2B_2$ symmetry around 15 eV but no evidence for the $^2A_1$ resonance around 6 eV.[11] Additional calculations which used the Schwinger multichannel variational method have been presented even more recently,[13] together with experimentally determined absolute integral cross sections.[13,14] The comparison involved differential cross sections at intermediate energies and the integral elastic cross sections from threshold up to 100 eV. They showed the presence of resonance features at different energies from those of the previous calculations and strong changes of its location when polarization forces were introduced. In another recent paper[15] the results of measurements and calculations of differential and integral cross sections for elastic electron scattering were presented as an extension of previous work by the same authors.[13]

In the present study we therefore intend to confirm and extend the analysis of resonance features within the different irreducible representations (IRs) which contribute to the total integral cross sections and further examine their behavior when the molecule is strongly distorted from its C_{2v} equilibrium geometry, along electronic energy landscapes which could describe the ensuing fragmentation channels of the temporary anions.

Section II outlines our computational scheme, while section III reports our results for the equilibrium geometry of CF_2. Section IV describes the changes in the resonance features when the molecule is distorted from its equilibrium geometry and discusses their relation with dissociative electron attachment (DEA) evolutionary pathways. The present conclusions are finally presented in section V.

II. THE COMPUTATIONAL METHOD: AN OUTLINE

II.A. Scattering Equations in a Single Center Expansion. In the Born−Oppenheimer (BO) approximation one represents the total wave function of the "target + e^-" as an antisymmetrized product of electronic wave functions which parametrically depend on the positions of the nuclei. The scattering process under investigation is here initially limited to elastic channels; therefore no electronic excitations are considered, and the N bound electrons of the target are assumed to be in a specific molecular electronic state (ground state) which is taken to remain unchanged during the scattering. The target electronic wave function is given by the self-consistent-field (SCF) approximation with a single determinant description of the N occupied molecular orbitals (MOs). In our scattering equations the occupied MOs of the target are expanded on a set of symmetry-adapted angular functions with their corresponding radial coefficients represented on a numerical grid.[16] In this approach, any arbitrary three-dimensional function describing a given electron, either a bound or a scattering electron, is expanded around the center of mass of the molecule, where the origin of the body-fixed frame is placed. The single-center expansion (SCE) is then given by

$$F^{p\mu}(r,\hat{\mathbf{r}}|\mathbf{R}) = \sum_{l,h} r^{-1} f_{lh}^{p\mu}(r|\mathbf{R})\, X_{lh}^{p\mu}(\hat{\mathbf{r}}) \tag{1}$$

where the indices refer to the μth component of the pth IR of the point group of the molecule at the nuclear geometry $\mathbf{R}$. The angular functions $X_{lh}^{p\mu}(\hat{\mathbf{r}})$ are symmetry-adapted angular functions given by the proper combination of harmonics $Y_{lm}(\hat{\mathbf{r}})$:

$$X_{lh}^{p\mu}(\hat{\mathbf{r}}) = \sum_m b_{lmh}^{p\mu} Y_{lm}(\hat{\mathbf{r}}) \tag{2}$$

The coefficients $b_{lmh}^{p\mu}$ are discussed in the literature and can be obtained from a knowledge of the character tables of the relevant molecular point group.[17] The coupled, partial integro-differential scattering equations take the form[16]

$$\left[\frac{d^2}{dr^2} - \frac{l(l+1)}{r^2} + 2(E-\varepsilon_\alpha)\right] f_{lh}^{p\mu\alpha}(r|\mathbf{R}) = 2 \sum_{l'h'p'\mu'\alpha'} \int dr'\, V_{lh,l'h'}^{p\mu\alpha,p'\mu'\alpha'}(r,r'|\mathbf{R})\, f_{l'h'}^{p'\mu'\alpha'}(r'|\mathbf{R}) \tag{3}$$

where E is the collision energy and ε_α is the electronic eigenvalue for the αth asymptotic state so that $k_\alpha{}^2/2 = E - E_\alpha$, where k_α is the asymptotic momentum of the electron with the target in a state α. The (p,μ,α) indices in eq 3 now label the symmetry and corresponding target state of the continuum wave function, and refer to the kernel of the integral operator $\hat{V}$, a sum of diagonal and nondiagonal terms that in principle fully describe the electron−molecule interaction during the collision. The choice of a single state α obtains the exact-static-exchange (ESE) representation of the electron−molecule interaction for the molecular ground state geometry $\mathbf{R}$. Introducing the further assumption of having only a local e^-−molecule interaction (as we shall also discuss below), one can again simplify the form of the coupled equations

$$\left[\frac{d^2}{dr^2} - \frac{l_i(l_i+1)}{r^2} + k^2\right] f_i^{p\mu}(r|\mathbf{R}) = \sum_j V_{ij}^{p\mu}(r|\mathbf{R})\, f_j^{p\mu}(r|\mathbf{R}) \tag{4}$$

where the indexes i or j represent the "angular channel" (l,h) and the potential coupling elements are given by

$$V_{ij}^{p\mu}(r|\mathbf{R}) = \langle X_i^{p\mu}(\hat{\mathbf{r}})|V(r|\mathbf{R})|X_j^{p\mu}(\hat{\mathbf{r}})\rangle = \int d\hat{\mathbf{r}}\, X_i^{p\mu}(\hat{\mathbf{r}})\, V(\mathbf{r}|\mathbf{R})\, X_j^{p\mu}(\hat{\mathbf{r}}) \tag{5}$$

In this study we model the exchange contribution to the operator of eq 5 with an energy-dependent local exchange potential suggested by Hara[18] and discussed by us many times before.[19] We further include the dynamical short-range correlation through the addition of a local energy-independent potential which is obtained by defining an average dynamical correlation energy of a single electron within the formalism of the Kohn and Sham variational scheme.[19] The functional derivative of such a quantity with respect to the SCF N-electron density of the molecular target provides a density functional description of the required short-range correlation energy as an analytic function of the target electron density.[16,19] The latter contribution is finally connected with the long-range dipole polarizability term providing the additional polarization potential contribution, as

given in detail in ref 16. The above modeling of the full interaction for an electron impinging on an many-electron target has been used by us many times before, finding rather good agreement with the available experimental data of several molecules.[16,19−22]

II.B. Adiabatic Potential Model. The main focus of this paper is on the mechanism and qualitative characteristics of possible low-energy, one-electron resonances and their evolutions along the various regions of the complex molecular potential energy surface (PES) landscape created by the nuclear motion of the temporary anion. This requires a model which is simple enough to be computationally attractive but which includes sufficient details of the full scattering problem to reproduce the essential features of the physics involved. Thus, we locate the low-energy resonances by using a simple, purely local model potential that we have called the static model-exchange correlation (SMEC) potential, V_{SMEC}.[16] We start by noting that the standard, symmetry-adapted angular momentum eigenstates, $X_{lh}^{p\mu}$, do not form the most compact angular set for the e$^-$−molecule scattering problem: an alternative basis expansion is provided, instead, by the angular eigenfunctions obtained by diagonalizing the angular Hamiltonian at each radius r. These distance-dependent angular eigenstates are referred to as the adiabatic angular functions (AAFs) $Z_k^{p\mu}(\theta,\phi,r)$ which, at each radial value, are linear combinations of the symmetry-adapted "asymptotic" harmonics discussed before:

$$Z_k^{p\mu}(\theta,\phi,r) = \sum_{lh} X_{lh}^{p\mu}(\theta,\phi)\, C_{lh,k}(r) \tag{6}$$

where the expansion coefficients are solutions of the matrix eigenvalue equation

$$\sum_{lh} V_{l'h',lh}(r)\, C_{lh,k}(r) = C_{l'h',k}(r)\, V_k^{\mathrm{A}}(r) \tag{7}$$

The eigenstates $V_k^{\mathrm{A}}(r)$ now form an adiabatic radial potential for each index k over the selected range of the e$^-$−molecule distances. The spatial extent of the resonant wave function can be determined from the well and angular momentum barrier of such adiabatic potential terms, and the physical mechanism for the resonance is that of a trapped electron tunneling through the potential barrier. In order to represent the nonadiabatic coupling terms between adiabatic curves, we actually employ a piecewise diabatic (PD) representation of the potential whereby the radial coordinate is divided into a number of regions so that sector i is defined as $r_{i-1} < r < r_i$, with $r_0 = 0$. In each radial region we average the coupling potential $V_{l'h',lh}(r)$ over r and the resulting averaged potential is diagonalized as in eq 7 to yield a set of angular functions $Z_{k,i}^{p\mu}(\theta,\phi)$. Then, in region i the scattering potential is transformed into the new representation in which it is nearly diagonal. The resulting equations are solved using the full scattering potential in each region with the further approximation of ignoring the off-diagonal couplings in that region: to solve the radial equations using the PD approach requires matching of the radial functions and their derivatives at the boundary between radial regions. The transformation of the radial functions from one region to the next is given by the transformation matrix $U_{k,k'}^{(i+1\leftarrow i)}$ defined by

$$U_{k,k'}^{(i+1\leftarrow i)} = \sum_{lh} C_{lh,k}^{(i+1)} C_{lh,k'}^{(i)} \tag{8}$$

When the size of the angular momentum eigenfunction basis used is larger than the size of the diabatic angular basis set, the transformation matrix $U_{k,k'}$ is not in general unitary. We accomplish the unitarization of $U_{k,k'}^{(i+1\leftarrow i)}$ using simple Gram−Schmidt orthonormalization on the columns of $U_{k,k'}^{(i+1\leftarrow i)}$. The above treatment, being easier in terms of computational cost, usually finds the resonances slightly shifted from those given by the full coupled-channel solutions of eq 4.[16] However, their nature and general features remain unchanged and of the same physical significance, while allowing for a reduction of the computational effort.

II.C. Resonance-Following Adiabatic Picture. As mentioned in the previous discussion, one of the aims of the present study is to model the evolution of the metastable anionic species which are formed by temporary electron attachment. We wish to present a description, at the molecular level, of the most likely fragmentation and/or stabilization paths which are followed by the initially bound molecular nuclei after coupling with the excess energy carried by the attached electron. In other words, we wish to present a realistic, albeit still approximate, description of the potential energy landscape of the complex PES over which the motion of the atomic partners of the metastable anion is taking place.[23] Because of the additional presence of the imaginary component of that PES, obviously related to the varying width $\Gamma(E_r;\mathbf{R})$ of the resonant compound state,[24] one common approach to the nuclear dynamics is the well-known "boomerang model" (e.g., see ref 25) whereby an additional component to the total potential is added in the form of $[-i\Gamma(E_r;\mathbf{R})]/2$,[26] and further employed in a time-dependent (TD) description of the nuclear motion for the metastable anion.[26]

In the present approach we shall be analyzing the evolution of the resonance features (i.e., energy location and width) from their initial detection for the molecular target at its equilibrium geometry through their changes along specific one-dimensional (1D) cuts of the multidimensional PES of complex energy. In addition, we will take advantage of the general effects of such pseudo-1D nuclear evolutions on the spatial modifications, within the region of the molecular configurations, of the resonant scattering wave function represented within the molecular space of the moving nuclei. We have performed similar studies on other polyatomic gases,[27,28] and we found that they provide, even before carrying out the TD dynamics for the metastable anions, a rather clear description, at the qualitative level, of the different channels which are more likely to be followed by the fragmentation of the initial metastable anion. Hence, the calculations described in the following will take advantage of various pieces of information obtained from scattering calculations over a broad range of molecular geometries: (i) the changes in space of the nodal structures and of the antibonding features of the resonant wave functions associated with the excess electron as the nuclear geometries evolve along a given coordinate; (ii) the changes of the resonant widths, $\Gamma(E_r;\mathbf{R})$, where $\mathbf{R}$ collectively describes the specific molecular geometry for which the resonance appears at the energy E_r.

$$E_r^{\mathrm{TNI}}(\mathbf{R}_i) = E_r(\mathbf{R}_i) + \frac{i\Gamma(\mathbf{R}_i)}{2} \tag{9}$$

where TNI labels the specific transition negative ion produced by the resonance in question.

We will further choose as an energy reference the value associated with the neutral molecular structure at the equilibrium geometry, $E_N^{\mathrm{A}}(\mathbf{R}_{\mathrm{eq}})$, with "A" labeling the specific IR for which the resonance appears. The corresponding electronic energy of the $(N+1)$-electron complex can therefore be obtained as

$$E_{N+1}^{\mathrm{A}} = E_r^{\mathrm{TNI}}(\mathbf{R}_i) + E_N^{\mathrm{A}}(\mathbf{R}_i) - E_N^{\mathrm{A}}(\mathbf{R}_{\mathrm{eq}}) \tag{10}$$

which will allow us to follow the electronic energy evolutions of the metastable states, TNIs, along specified selected cuts of the multidimensional PES landscape and for a selected resonance, in conjunction with the corresponding spatial changes of the excess electron scattering wave function and of its lifetime (width).

III. RESONANCE FEATURES AT THE EQUILIBRIUM GEOMETRY

The properties of CF_2 at the equilibrium geometry were the subject of several papers from both theoretical[29−38] and experimental[38−45] viewpoints. The geometry of its ground state was studied spectroscopically in the microwave[39,40] and infrared[41,42] regions, and structural parameters of the ground state have been derived from absorption spectroscopy.[45] According to these studies, the CF_2 molecule belongs to the C_{2v} symmetry group and the most recent experimental values derived from the rotational constants (see ref 38 and references therein for a thorough comparison with earlier results) for the C−F bond length and for the F−C−F angle are 1.2975 Å and 104.81°, respectively. The existing ab initio calculations on the geometry of CF_2 are also in good agreement with these experimental findings: the best theoretical values (see ref 36 and references within for a state-of-art, ab initio description of the CF_2 molecule) gave r_{CF} = 1.2972 Å and $\theta_{\angle FCF}$ = 104.858°.

To get the target molecular orbitals (MOs), our calculations employed a conventional representation over a Gaussian basis set and the quality of the expansion was given by a D95* expansion.[27] The bond length initially employed for the equilibrium geometry was 1.283 Å.[18] The size of the physical "box" that contains the diabatized potential terms described before was 15 Å, and the overall radial and angular grids (r,ϑ,φ) included 1300 × 84 × 324 points. The single-center expansion for the potential was checked for convergence on the final cross sections and included terms up to λ_{max} = 50. Likewise, the corresponding partial wave expansion for the scattered electron was carried out up to l_{max} = 100. The calculated wave function for the neutral target yielded a permanent dipole moment value of μ_{eq} = 0.60 au, not far from experiments,[22] as mentioned before.

The data of Figure 1 show the calculated rotationally summed, integral cross sections (ICSs) for all four IRs contributing to the ground state scattering process from the C_{2v} molecule in its equilibrium geometry. Three of the partial ICSs shown in Figure 1 exhibit resonant scattering features: below 1 eV in the $^2B_1$ symmetry, and around 11−12 eV as broader resonances for the $^2A_1$ and $^2B_2$ anionic states. Earlier calculations[11,12,15] predicted a significant resonance enhancement of the elastic integral total cross sections (ITCSs) at low energies and a broader resonance at higher energies, although the peak appears at different energies in each of the above studies: the calculations of ref 15 predict its occurrence at energy below ∼0.1 eV, while the distorted wave (DW) calculations of ref 12 find it around 1.6 eV. The *R*-matrix[11] calculations, however, locate that resonance at ∼0.70 eV, i.e., in agreement with two of the earlier calculations[11,15] which place that resonance around or below ∼1.0 eV. Unfortunately, the experimental data do not extend below 2.0 eV[13,14] and therefore cannot yet provide an unequivocal assignment of the resonance position. It is interesting to further note, however, that the adiabatic electron affinity (EA) experimentally determined[34] indicates a positive value of 0.18 ± 0.02 eV for a stable CF_2^- anion of $^2B_1$ symmetry. Our calculated resonance is indeed of that symmetry (see Figure 1) and describes, as we shall see later, a metastable anion with a very small (negative) electron affinity, which indicates an anionic state that is very nearly bound at that vertical geometry and that requires a rather small internal rearrangement of the nuclear vibrational content of that resonance in order to become the bound anion of that symmetry. This aspect of the resonance evolution will be further discussed below.

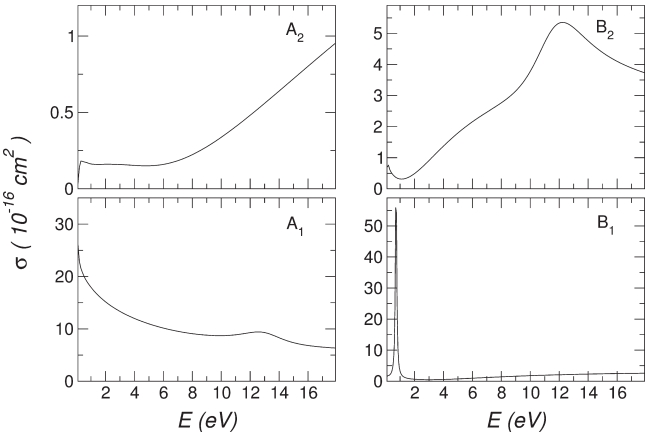

Figure 1. Partial integral cross sections computed for the C_{2v} equilibrium geometry of $CF_2(X^1A_1)$ as a function of electron scattering energy.

The previous calculations[12,15] additionally locate two, much weaker, resonances of a_1 and b_2 symmetries, corresponding to metastable anionic formation of $^2A_1$ and $^2B_2$ symmetries: our calculations in Figure 1 indeed confirm such findings. The $^2A_1$ resonance was found at about 12 eV in ref 15, rather close to our calculation at 11.84 eV. The one of $^2B_2$ symmetry was located at about 13.5 eV in ref 15 and at about 15 eV in ref 12: our present results place that resonance around 11 eV, i.e., only qualitatively close to the previous findings. In conclusion, all existing calculations on this system, including ours, indicate the presence of three resonances in the B_1, B_2, and A_1 IRs of the equilibrium molecular geometry, with the first being very close to threshold and much more narrow than the other two.

We have mentioned in section II that the spatial mapping of the resonant wave functions for the scattered electrons over the nuclear configurations of the target molecule can provide useful pictorial indicators on the expected properties of that resonant state and also show us the region of antibonding character which they add to the existing electronic density distributions of the bound *N* electrons.[27]

The panels of Figure 2 report the calculated maps of the excess, resonant electrons at the three IRs discussed before, together with their energy position, E_r, and the $\Gamma_r/2$ value (in electronvolts). The following features of the metastable states can be gleaned from the pictures reported in Figure 2:

(i) The $^2B_1$ anion, as mentioned before, describes a metastable precursor to the stable anionic configuration: the π^*-like character of it is shown by the clear symmetry plane that contains the molecular nuclei, by the antibonding planes across both C−F bonds, and by the strong π^* character of the density regions over each of the three atoms.

(ii) Both resonances at the higher energies show, instead, a marked σ^* character and density distributions that reside chiefly along the two CF bonds, with the presence of clear antibonding features across them.

(iii) The $^2A_1$ resonant wave function (right panel of Figure 2) further indicates the presence of a substantial portion of

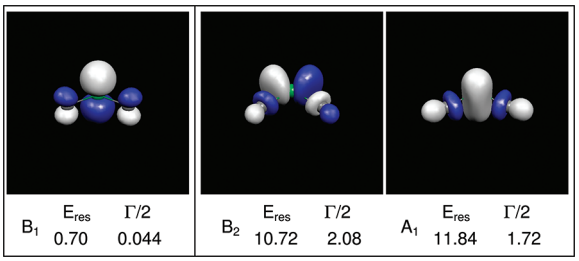

Figure 2. Computed electron wave function maps for excess electrons of the three resonances found for CF_2 at R_{eq}. The energy locations, E_{res} (in electronvolts), and resonance widths, $\Gamma/2$ (in electronvolts), are also shown. See text for further details.

the excess charge on the C atom, with smaller portions on the two F atoms. On the other hand, the $^2B_2$ resonant wave function places most of its excess charge along the bonding regions, with less of it on any of the three atoms.

Such initial structural differences between the spatial features of the resonant electrons shall have a role in guiding the different fragmenting pathways of this molecule, as will be described in section IV.

IV. RESONANCE EVOLUTIONS ON BOND DEFORMATIONS

As discussed in section II, our present computational approach allows us to employ a variety of "indicators", generated by quantum multichannel scattering calculations, which can help us in following the evolution of each of the previously located resonances as one stretches or bends one or more of the molecular bonds. More specifically, the construction of pseudo-1D cuts of the complex potentials supporting the nuclear structures of the metastable anions will show us the evolution of the energy locations and of the associated lifetimes of the resonances, while the corresponding maps of the excess electron wave functions will further help us in qualitatively understanding the likely paths to dissociative attachment channels. Thus, short of actual dynamical calculations for the nuclear motion, the present computed "indicators" already allow us to draw some significant conclusions of the anionic stabilization process.

IV.A. Symmetric Bond Stretching. The simplest bond deformation is that where the C_{2v} symmetry is preserved and the bonds are stretched simultaneously, bringing the two F atoms away from the central carbon atom. The results of our calculations are shown by the three panels of Figure 3.

The top panel of Figure 3reports the shifting of the resonance position and width, for the IR component $^2B_1$, as the bond length is both shortened (to 1.15 Å) and lengthened (to 1.35 Å). In the latter case, one clearly sees that the energy location of the metastable anion moves closer to the energy threshold and also acquires a much narrower width (i.e., a longer lifetime).

This behavior is more clearly seen in the plot of the middle panel of Figure 3, where we report the actual values of the $^2B_1$ resonance over a broader range of bond stretching values, together with the values of the associated widths for each of the resonance calculations at that geometry. The results indicate that, as the bonds stretch beyond their equilibrium values, while keeping the C_{2v} symmetry, the resonance becomes narrower in width and much closer to the zero energy of the system.

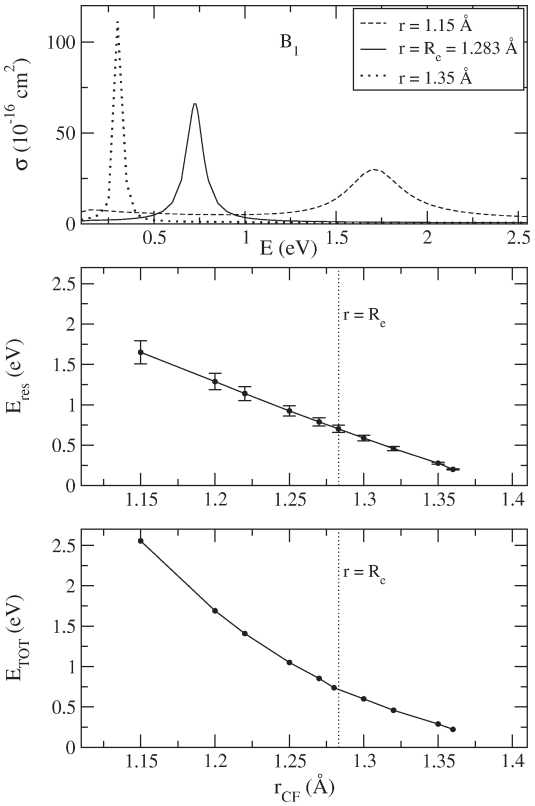

Figure 3. Partial integral cross sections computed in the C_{2v} geometry by symmetrically stretching both C−F bonds. Top panel: shift of the width and position of the $^2B_1$ resonant state for three representative bond lengths. Middle panel: resonant energy displacement on bond stretching. The bars for each point of the curve show the resonance width values. Bottom panel: real part of the total energy of the metastable $(N + 1)$-electron target as a function of the bond length values.

Another pictorical view of the behavior of this resonance is given by the bottom panel of Figure 3. We report there the real part of the total electronic energy of the metastable anion, defined by eq 10, as a function of bond stretching within the C_{2v} geometry. The potential reported there describes the Born−Oppenheimer (BO) PES's cut along a pseudo-1D direction for the metastable anion. It is shown that the system moves down to crossing the corresponding PES of the N-electron system (which has its E = 0.0 value at the R_{eq} position shown by the vertical dotted line) at a bond distance of about 1.40 Å. It is interesting to note that earlier ab initio calculations for the stable anion of $^2B_1$ symmetry[37] found that its minimum energy structure was for R_{eq} ∼1.438 Å and close to the experimental estimate of 1.45 ± 0.02 Å .[43] A smooth extrapolation of our scattering results into the bound-state region suggests a bond length of ∼1.44 Å in good agreement with the above data. Furthermore, the bond angle we used was the θ_{eq} = 104.73° while the estimates[37,43] for the stable anion are around 100°. Thus, the pure stretching "cut" of the present PES is still an approximate view that is already providing the correct result. One should further note that the present findings are also in agreement with the R-matrix calculations of ref 6.

Additional pictorial help from the spatial features of the scattering wave function at the resonance is given by the data in the two panels of Figure 4.

We show in Figure 4 the resonant electron wave function at both the R_{eq} value and for a stretched configuration: no apparent

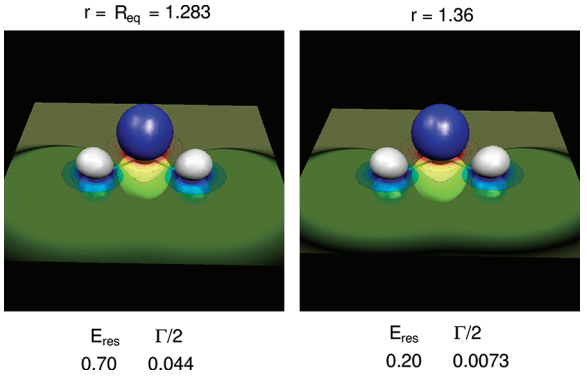

Figure 4. Three-dimensional representation of the scattering resonant wave function of the $^2B_1$ metastable anion at two different bond length values (in angstroms). The widths and positions of the resonances (in electronvolts) are reported below each panel.

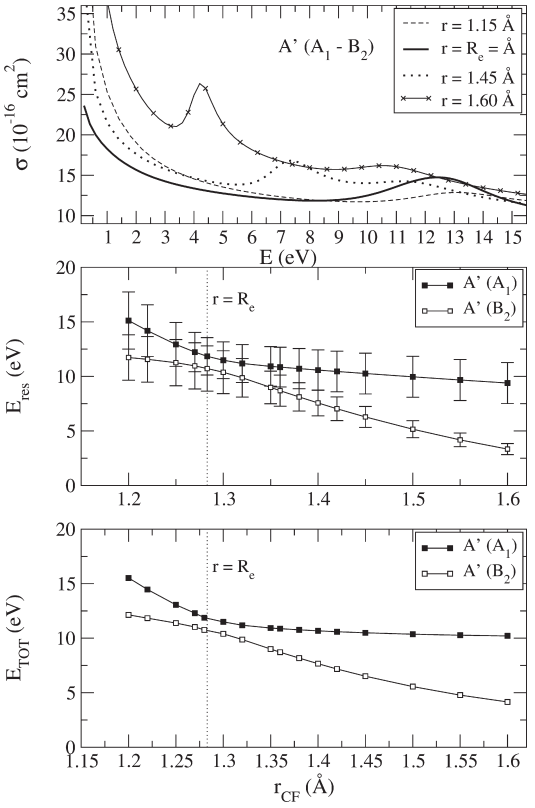

Figure 5. Effects of asymmetric bond stretching on the $^2A_1$ and $^2B_2$ σ^*-like resonances. Top panel: behavior of the partial ICS of $^2A_1$ symmetry as one of the two C−F bonds is stretched. Four representative values are reported. Middle panel: behavior of each separate resonance ($^2A_1$ and $^2B_2$) position and width upon asymmetric stretching. Bottom panel: Born−Oppenheimer computed PES cut along the single bond stretching for both metastable anions (real part). See text for further details.

change in shape and delocalization of the scattered electron is seen to occur, an indication of the fact that the stretched molecule is evolving along this pathway into a stable anion of $^2B_1$ symmetry having strong π^*-like characteristic and essentially delocalized over the whole molecule.

The behavior of the other two σ^*-like resonances ($^2A_1$ and $^2B_2$), when analyzed under symmetric stretching of the nuclear

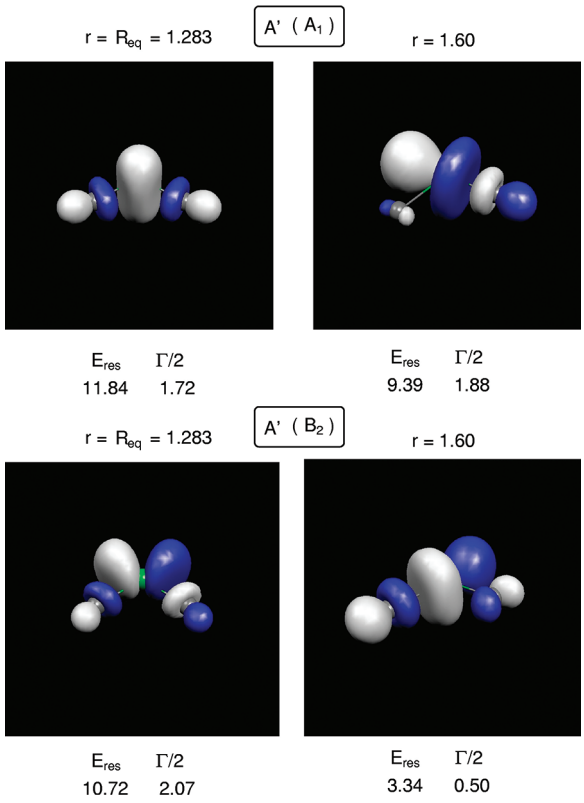

Figure 6. Computed three-dimensional views of the resonant electron wave functions for the initial $^2A_1$ (upper panels) and the $^2B_2$ (lower panels) resonances as one of the CF bonds is stretched. The bond length values are in angstroms and the widths and positions of the resonances are in electronvolts. See text for further details.

geometry, is such that it leaves each TNI as unchanged: we indeed do not observe any variation in both the resonance energy position and in the corresponding resonance width.

IV.B. Asymmetric Bond Stretching. Another possible, and chemically interesting, pseudo-1D cut of the multidimensional PES for the metastable anion is provided by stretching asymmetrically the two CF bonds. We therefore kept one of them at its R_{eq} value while stretching the other bond, thereby destroying the C_{2v} symmetry. Our calculations at R_{eq} reported in the previous section indicated, in the region around 10−12 eV, the presence of two fairly broad σ^*-like resonances of $^2A_1$ and $^2B_2$ symmetry, respectively.

The experimental data[6,46] indicate thresholds for formation of C^- + F_2 to occur above about 7.7 eV and that for F_2^- + C to occur around 6 eV. The F^- peak is observed[46] as a threshold peak and also with a maximum around 0.95 eV.[6] The thermodynamic threshold peak for the formation of CF^- should be above 5.20 eV,[46] and so should be the one for F^-.[46] All four negative fragments could therefore be formed in an energy region between 5 and 8 eV. The experiments actually observed the F_2^- signal around 2.8 eV and, as mentioned above, the F^- peak close to threshold. Fast atom reactions[46] also yielded F^- formation from CF_2.

The present calculations on the behavior of the two σ^*-like resonances are reported in the three panels of Figure 5.

The top panel of Figure 5 shows the behavior of both resonances (which are now A′ resonances for the distorted geometries) coming from the stretched and compressed bonds.

dx.doi.org/10.1021/jp206618x |J. Phys. Chem. A 2011, 115, 11531–11543

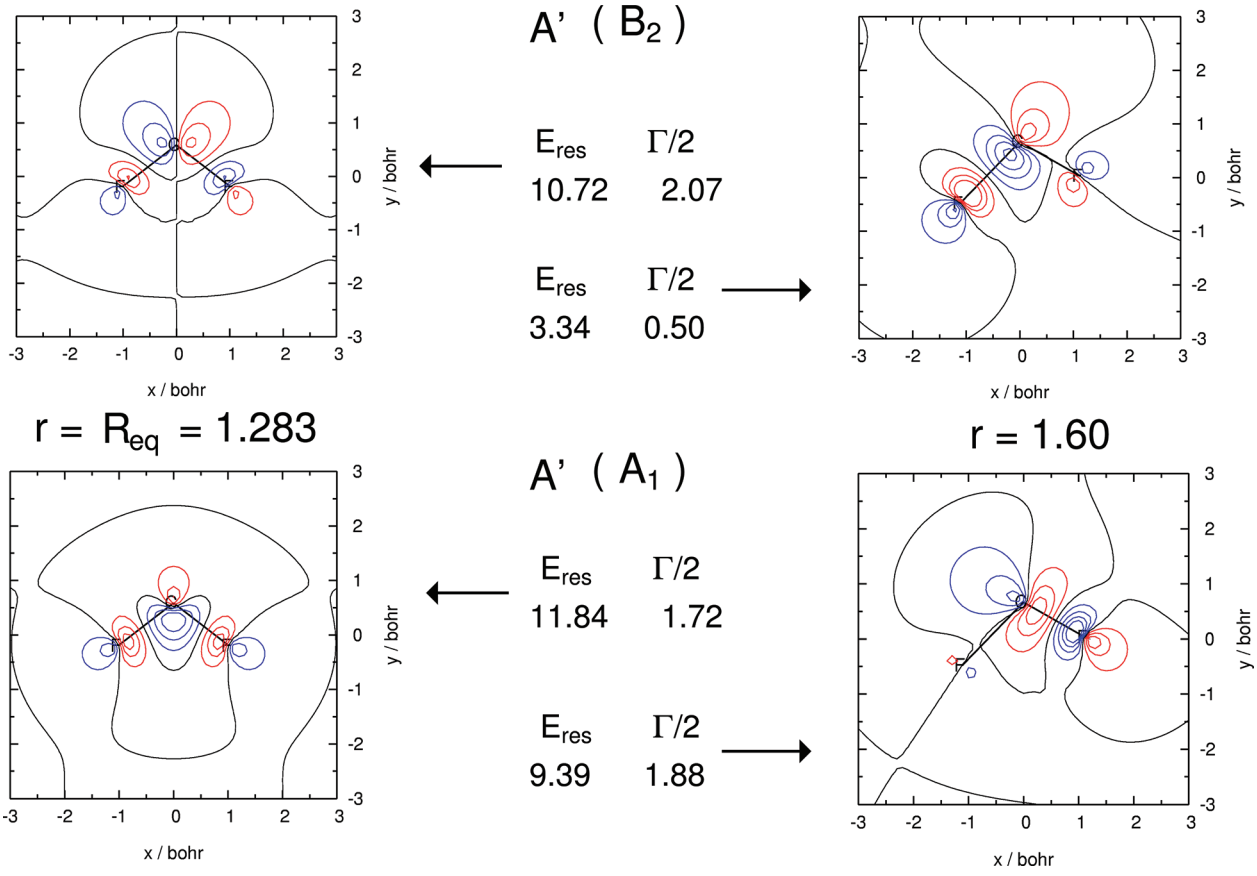

Figure 7. Computed two-dimensional maps of the scattering, resonant wave functions of $^2B_2$ (upper panels) and $^2A_1$ (lower panels) for symmetric (left) and asymmetric (right) bond configurations.

Due to the marked differences in size of the partial ICS values (see data of Figure 1), only one of them is actually shown. A more detailed analysis of the relative behavior for both resonances is shown by the middle panel of Figure 5, where their positions and widths, following the same notation as Figure 3, are reported for a range of single-bond stretching.

Both resonances are seen to decrease in energy, while the $^2B_2$ resonance shows much stronger lowering of its energy location and a much more marked narrowing of its width, i.e., a marked increase of its lifetime.

The bottom panel of Figure 5 finally shows the energy path of the real parts of the PESs for the $(N + 1)$-electron metastable anions: the presence of an avoided crossing at nuclear geometries just beyond their locations at equilibrium is clearly visible. In terms of diabatic behavior, therefore, one could suggest that the two σ^* resonances, which belong to different IRs at the R_{eq} geometry of CF_2, are now degenerate within the A′ PES and therefore the neutral $^2A_1$ resonance can diabatically evolve as a dissociative $^2A'$ resonance with $^2B_2$-like features after the crossing. The same, but in reverse order, is occurring for the $^2B_2$ resonance: we shall further discuss this point below.

A pictorial analysis of such a behavior could be had by looking at the panels of Figures 6 and 7, where maps of the resonant wave functions are shown under asymmetric bond stretching deformations.

The three-dimensional maps of the scattering wave functions for the excess electron in both resonances, reported in the panels of Figure 6, show an interesting spatial evolution for the shape of the resonant electron: the $^2A_1$ indicates that the excess electron becomes localized on the C−F bond which is *not* being stretched with most of its density on the C atom (upper right panel of Figure 6), while its lifetime does not increase much (middle panel of Figure 5), thereby indicating that the temporary (CF^-) anion is very likely to decay by electron detachment before the full dissociative path along the other bond progresses to the asymptotic region.

On the other hand, the $^2B_2$ resonance follows a different evolution: the resonant electron becomes preferentially localized along the stretched bond, keeps a substantial part of its density over the F atom which is moving away, and exhibits a marked antibonding character along that bond. If one combines these findings with the marked increasing of the lifetime of this resonance as one F atom is stretched (see middle panel of Figure 5), then it seems reasonable to expect that the evolution of the $^2B_2$ resonance on asymmetric bond stretching would be the asymptotic fragmentation into F^- + $CF(^2\Pi)$, as suggested by both earlier calculations[6] and the more recent experiments.[46]

The possible resonance evolution outlined in the previous discussion becomes even clearer when the two-dimensional maps of the scattering electron wave functions are examined in the region of the nuclear configurations, as shown by the panels of Figure 7.

We report in the two panels on the left of Figure 7 the contour lines of the scattering wave functions for the two resonances at the R_{eq}: one sees clearly the strong localization of the wave function on the C atom for the $^2B_2$ resonance and the greater distribution of the latter along the bonds and terminal F's for the $^2A_1$.

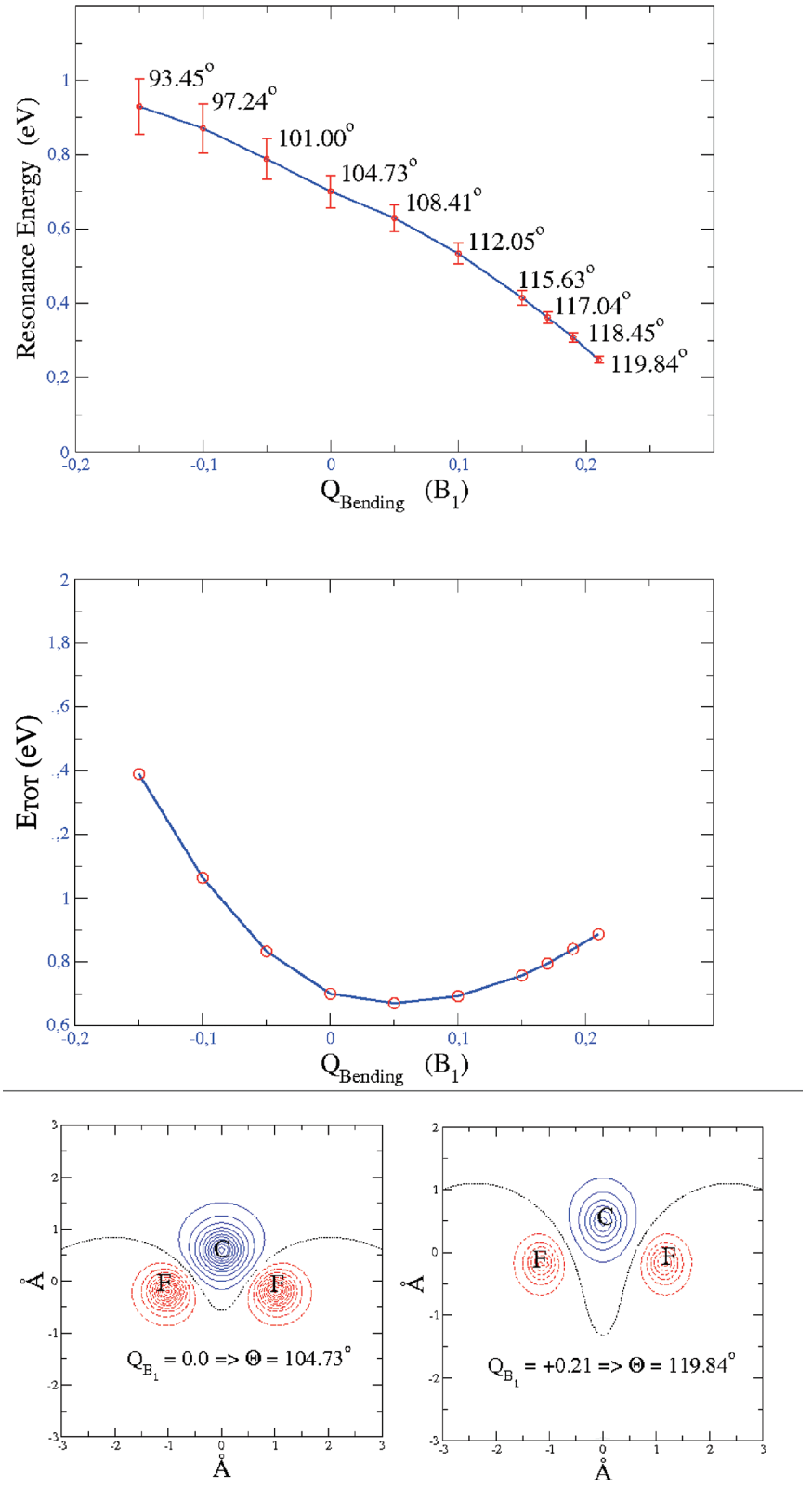

Figure 8. Top panel: resonance evolution for the $^2B_1$ metastable anion upon bending. The actual angle values are given at each point. Middle panel: total electron energy, real part, for the $(N + 1)$-electron $^2B_1$ metastable anion on bending motion. Bottom panel: contour lines for the computed electron resonant wave functions at two different angles. See text for further details.

The contour lines at the stretched, asymmetric geometry (panels on the right in Figure 7) show instead the different evolutions of the two resonances: the $^2B_2$ is now localized along the stretched bond and the receding F atom, while the $^2A_1$ wave

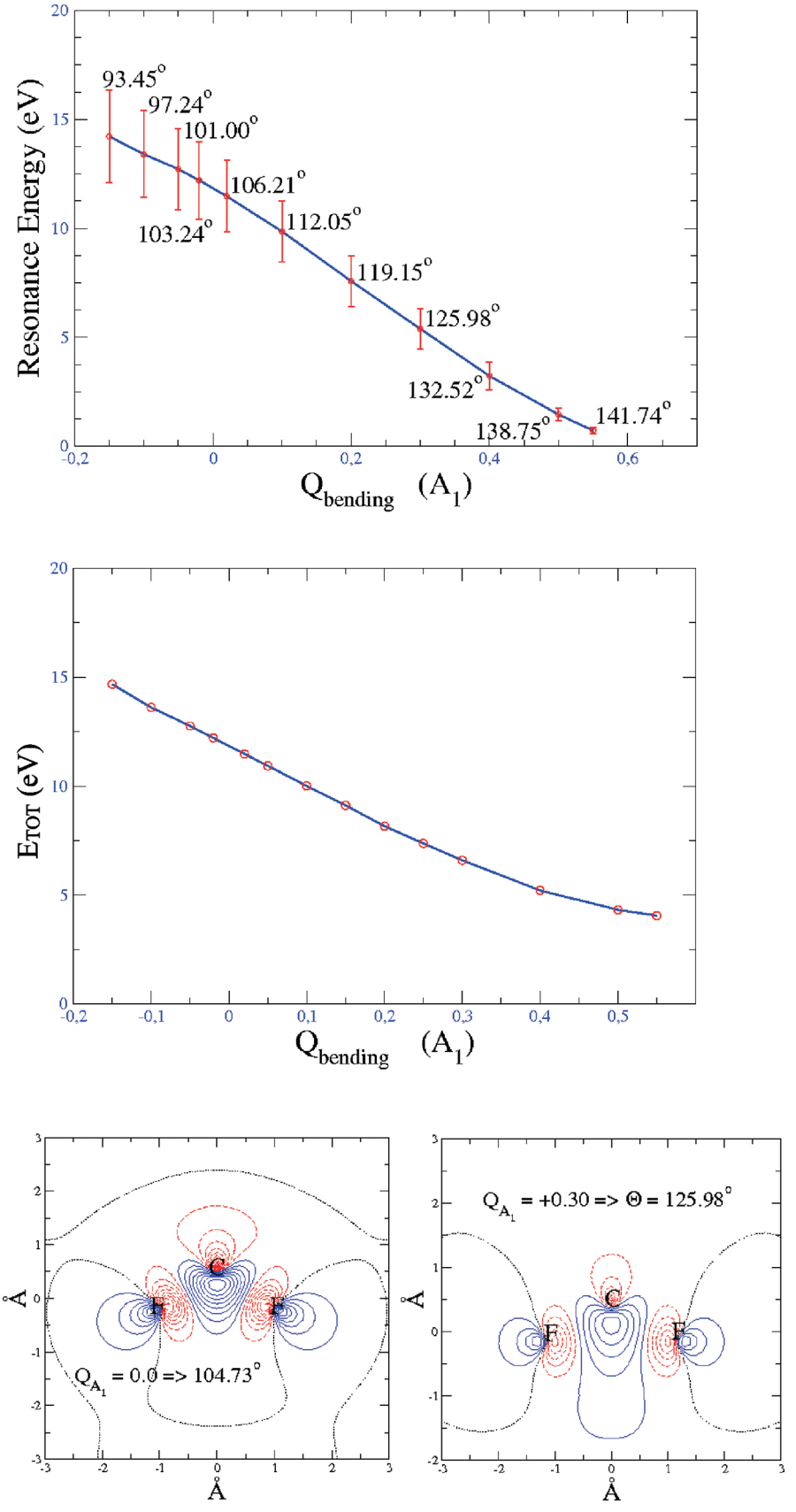

Figure 9. Same as in Figure 8, but for the $^2A_1$ σ^*-like resonance. See text for further details.

dx.doi.org/10.1021/jp206618x |*J. Phys. Chem. A* 2011, 115, 11531–11543

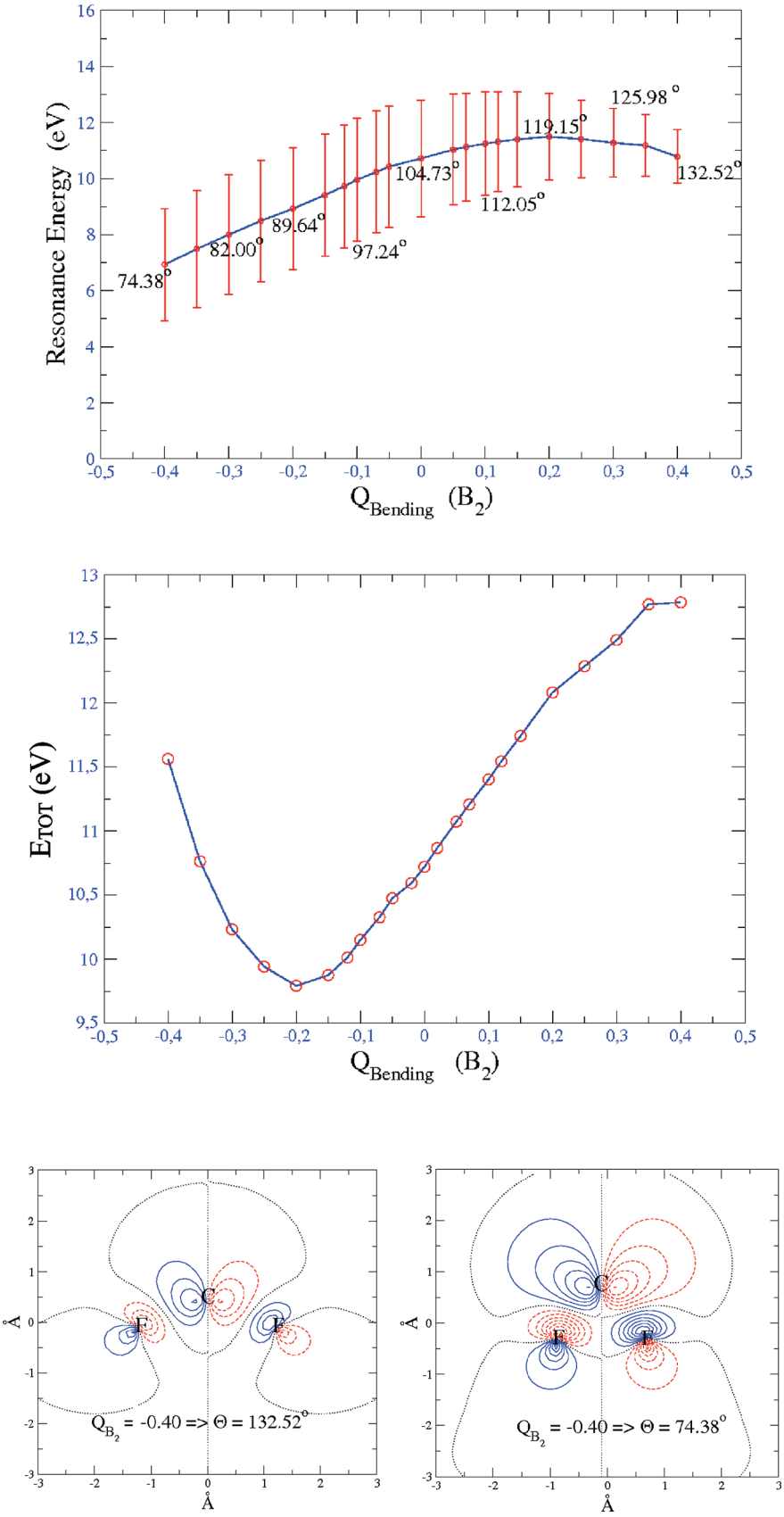

Figure 10. Same as in Figures 8 and 9, but for the $^2B_2$ σ^*-like resonance. See text for further details.

function remains on the unchanged bond and localized on its C−F region. Its width is also largely unchanged, indicating no increased stabilization of that metastable anionic fragment, in contrast to the $^2B_2$ resonance where the lifetime of the metastable F^- fragment is markedly increased (see upper panels in Figure 7).

In conclusion, the asymmetric stretching, pseudo-1D evolutionary paths for the $^2A_1$ and $^2B_2$ resonances suggest a diabatic evolution from the initial $^2A_1$ into a stabilized $^2A'$ ($^2B_2$) fragmentation producing F^-, while the initial $^2B_2$ also evolves diabatically into a $^2A'$ ($^2A_1$) metastable state, this time with CF^- features but without stabilization of the latter; this system, therefore, is likely to evolve into electron detachment that would prevent observation of a stabilized CF^- asymptotic anion, as is indeed indicated by the experiments.[46]

IV.C. Bending the F−C−F Angle. As initially discussed, the C_{2v} equilibrium configuration of difluoromethylene has an angle of 104.73° between its two C−F bonds. In the present section we follow the three resonances discussed in sections IV.A and IV.B to observe the effect on them from angle deformations.

The panels in Figure 8 report the changes in energy locations and resonance widths which occur for the π^*-like resonance discussed in section IV.A, the $^2B_1$ metastable anion. The top panel in Figure 8 clearly indicates that the threshold resonance moves further down in energy and becomes much more stable. The corresponding real part of the PES's cut of $^2B_1$ symmetry, shown in the middle panel of Figure 8 , further confirms the stable structure of the deformed anion and its minimum energy at a slightly larger angle of ∼107°. Finally, the isolines for the corresponding scattering wave function in the bottom panels of Figure 8 indicates the essential invariance of this π^*-like resonance when the angle is increased: the excess charge coming from the scattered electron remains localized over the three atoms, while the energy stabilization seen above indicates that the formation of a stable $CF_2^-(^2B_1)$ chiefly occurs by the previously discussed symmetric stretching, with the bending contributing to its stabilization only for small deformations of θ. The resonance, therefore, is confirmed to be the one yielding the stable anionic species, with rather limited structure deformations from the (R_{eq}, θ_{eq}) configuration.

The consequences of the bending deformation on the evolution of the two remaining resonances, i.e., the σ^*-like resonances of $^2A_1$ and $^2B_2$ symmetries, are reported in Figures 9 and 10, respectively.

The evolution of the $^2A_1$ resonance, already discussed before when undergoing asymmetric stretching deformations, shows clearly from the top panel of Figure 9 that its energy location dramatically decreases down to the energy threshold upon increasing the θ angle, while the associated width also becomes much narrower. The corresponding real part of the total energy for the $(N + 1)$-electron system in that symmetry is reported by the middle panel of Figure 9. That particular cut of the multidimensional PES is seen to be clearly dissociative in the sense that the overall anionic energy decreases when θ increases. A possible consequence of this dissociative stabilization could be gleaned by looking at the scattered wave function isolines shown by the bottom panels of Figure 9: the angle deformation of this symmetry creates charge localization from the excess electron onto the outer F atoms, with strong antibonding planes across both C−F bonds. Combined with the lifetime increase observed in the top panel and the dissociative shape of that pseudo-1D path (middle panel), this result suggest that F^- formation from either terminal atom is a likely evolution path for this resonance upon bending deformation of its atomic components.

The evolution of the $^2B_2$ σ^*-like resonance is shown by the various panels reporting our calculations in Figure 10. The calculations given in Figure 10 reveal, as was the case for the asymmetric stretching analysis, a very different behavior of the present resonance with respect to the other, σ^*-like resonance. The top panel of Figure 10 shows, in fact, that the $^2B_2$ energy position moves up from θ_{eq} as the angle is enlarged, while coming down in energy as the θ angle is reduced; in both ranges, however, the widths associated with that resonance remain rather large and indicate fairly short attachment times.

The energy trend is further seen by the cut along the bending coordinate of the electronic PES, real part, for the $(N + 1)$-electron metastable anion (middle panel of Figure 10). The energy minimum of the latter is located at a much smaller θ value with respect to the equilibrium for the neutral species: θ_{min} in Figure 10 is around 80° and the potential cut has no dissociative feature in that pseudo-1D representation. This resonance does not lead to dissociation and does not become more long-lived as θ is varied.

The bottom panels of Figure 10 further show the isolines describing two-dimensional mappings of the resonant wave function associated with the $^2B_2$ state, for different values of the bending angle. The θ_{eq} structure shows the known behavior of that resonance: excess electronic density onto the C atom and also along the C−F bonds. As the angle is reduced, however, we see there that the two F atoms get closer to one another and the excess electronic density moves onto those terminal atoms with marked antibonding planes across both bonds. Such behavior could indicate, given the lowering of the corresponding resonance position as θ is reduced (top panel in Figure 10), that the present resonance would tend to stabilize a longer-living transient $(F_2^-)^*$ anion. However, given the permanence of overall short lifetimes of such an anion, one would expect here that autodetachment of the metastable electron would occur before asymptotic formation of a stable F_2^- product.

In conclusion, the evolution of the $^2B_2$ resonance upon bending deformation could lead to the formation of F_2^- only if additional, multidimensional intramolecular vibrational redistribution (IVR) pathways would succeed in stabilizing it after this initial step: the experiments indicate[46] that the F_2^- formation should in fact be a minor dissociative channel for CF_2.

V. PRESENT CONCLUSIONS

The computational work discussed in this paper has analyzed in detail the evolutions of the three different metastable anions of the CF_2 molecule in the gas phase. The calculations have been carried out using a multichannel quantum scattering approach and have employed a parameter-free modeling of all the interaction forces acting between the molecule and the low-energy impinging electron. The study has been limited to the ground electronic state of the target molecule, and therefore only single-channel dynamical resonances have been considered in the analysis.

The molecular geometries have involved the structure deformations associated with the symmetric stretching, asymmetric stretching, and bending modes of the molecule: the initial three resonances of $^2B_1$, $^2A_1$, and $^2B_2$ symmetries detected for the CF_2 in its equilibrium geometry have been adiabatically followed along the corresponding PES for each of the modes, selecting

however a pseudo-1D representation of each normal mode in order to simplify the calculations.

The ensuing, complex electronic PESs for all three resonances have been analyzed for all three modes and the following results have been gleaned from a very broad range of calculations:

(i) Symmetric stretching mode: The threshold energy resonance of $^2B_1$ symmetry turns out to be markedly stabilized into a very narrow width (long lifetime) metastable species very close to zero energy, where the excess electron mantains its initial π^*-like character and is distributed always over the three atomic regions. In other words, the symmetric stretching deformation describes the passage of the $^2B_1$ metastable anion into a bound $^2B_1$ anion only 0.75 eV below the position of the neutral, as is also experimentally suggested.[6,46]

(ii) Asymmetric stretching mode: The effect of this deformation on the two σ^*-like resonances of $^2A_1$ and $^2B_2$ symmetry is to cause for both of them marked lowering of their energy locations (initially around 10−12 eV, see Figure 1). However, the reduced symmetry of the system brings both resonances to be of A′ symmetry and their corresponding electronic PESs for the two different metastable anions undergo an avoided crossing close to the equilibrium geometry (see middle panel in Figure 5). In other words, an electron attached to the difluoromethylene molecule in the A_1 IR at equilibrium will create a metastable state which can adiabatically evolve into a final $A'(B_2)$ resonance that moves down in energy as the asymptotic stretching occurs and acquires a much longer lifetime. The mapping of the corresponding excess electron wave function for the metastable state shows that it acquires localization onto the stretching CF bond and onto the terminal F atom. It is therefore reasonable to assume this motion to be responsible for the production, at low energies, of F^- atoms, as is experimentally observed.[46]

On the other hand, the $^2B_2$ resonance at the equilibrium geometry diabatically evolves into a final $A'(^2A_1)$ metastable state that does not stabilize much in energy or acquire narrower widths. The corresponding mapping shows localization of the latter on the unchanged C−F region: temporary formation of CF^- which, however, is likely to undergo autodetachment before stabilization. No CF^- fragments seem to have been experimentally observed.[46]

(iii) Bending mode: All three resonances have been analyzed under deformations of the F−C−F molecular angle θ, and it was found that the $^2B_1$ threshold resonance led again to stabilization of the $^2B_1$ bound anion at angular values slightly distorted from the equilibrium of ∼104°. On the other hand, the two higher energy σ^* resonances behave differently from one another, with the $^2A_1$ resonance evolving into a long-lived metastable anion which goes markedly down in energy along a pseudo-1D dissociative path as θ is increased. An analysis of its excess electron wave function indicates formation of F^- along this dissociative path, as is indeed observed in experiments.[46]

The $^2B_2$ resonance, on the contrary, does not show any dissociative features of its electronic PES cut for bending coordinate, nor does it exhibit any markedly longer lifetime of the resonance. It indicates, instead, that geometries with a reduced θ value show excess electron density moving over the two F atoms, now closer to one another and with antibonding features along both C−F bonds. Thus, it may give rise to a metastable intermediate of F_2^- which needs some further mechanism to be asymptotically stabilized: observations[46] indicate a negligible presence of this fragmentation product.

In conclusion, the present quantum scattering calculations on the evolutions of the resonant electron attachments to CF_2, as the molecule is deformed from its equilibrium structure, indicate specific fragmentation paths which stabilize, in the main, either a slightly deformed CF_2^- anion or the F^- fragment. Both agree with what has been experimentally found, while the present analysis provides physical reasons for the above results and rationalizes the experimental findings.

AUTHOR INFORMATION

Corresponding Author

*E-mail: fa.gianturco@caspur.it. Fax +39-06-49913305.

ACKNOWLEDGMENT

We are grateful for financial support from the 2006 PRIN project, the University of Rome "Sapienza" Research Committee, and a CASPUR Consortium Computational grant allowing us to complete the present project

REFERENCES

(1) Makabe, T. *Adv. At., Mol., Opt. Phys.* **2001**, *44*, 127–154.
(2) Special Issue: "Plasma Physics and Technology". Becker, K. H. *Eur. Phys. J. D* **2009**, *54*, 139.
(3) Special Issue: "Microplasmas, Challenges and Technological Opportunities". Becker, K. H.; Kersten, H.; Hopwood, J.; Lopez, J. L. *Eur. Phys. J. D* **2010**, *60*, 437.
(4) Matsuura, T.; Honda, Y.; Murota, J. *Appl. Phys. Lett.* **1999**, *74*, 3573–3575.
(5) Matsuura, T.; Murota, J.; Sawada, Y.; Ohmi, T. *Appl. Phys. Lett.* **1993**, *63*, 2803–2805.
(6) Rozum, I.; Limão-Vieira, P.; Eden, S.; Tennyson, J.; Mason, N. J. *J. Phys. Chem. Ref. Data* **2006**, *35*, 267–284.
(7) Tarnovsky, V.; Kurunczi, P.; Rogozhnikov, D.; Becker, K. *Int. J. Mass Spectrom.* **1993**, *128*, 181–194.
(8) Deutsch, H.; Becker, K.; Matt, S.; Märk, T. D. *Int. J. Mass Spectrom.* **2000**, *197*, 37–69.
(9) Joshipura, K. N.; Vinodkumar, M.; Antony, B. K.; Mason, N. J. *Eur. Phys. J. D* **2003**, *23*, 81–90.
(10) Rozum, I.; Tennyson, J. *J. Phys. B: At. Mol. Opt.* **2004**, *37*, 957–966.
(11) Rozum, I.; Mason, N. J.; Tennyson, J. *J. Phys. B: At. Mol. Opt.* **2002**, *35*, 1583–1591.
(12) Lee, M.-T.; Iga, I.; Machado, L. E.; Brescansin, L. M.; y Castro, E. A.; de Souza, G. L. C. *Phys. Rev. A* **2006**, *74*, 052716.
(13) Maddern, T. M.; Hargreaves, L. R.; Francis-Staite, J. R.; Brunger, M. J.; Buckman, S. J.; Winstead, C.; McKoy, V. *Phys. Rev. Lett.* **2008**, *100*, 063202.
(14) Maddern, T. M.; Hargreaves, L. R.; Bolorizadeh, M.; Brunger, M. J.; Buckman, S. J. *Meas. Sci. Technol.* **2008**, *19*, 085801.
(15) Francis-Staite, J. R.; Maddern, T. M.; Brunger, M. J.; Buckman, S. J.; Winstead, C.; McKoy, V.; Bolorizadeh, M. A.; Cho, H. *Phys. Rev. A* **2009**, *79*, 052705.
(16) For example, see: Lucchese, R. R.; Gianturco, F. A. *Int. Rev. Phys. Chem.* **1996**, *15*, 429–466.
(17) Altman, S. L.; Herzig, P. *Point-Group Theory Tables*; Oxford University Press: Oxford, U.K., 1994.
(18) Hara, S. J. *J. Phys. Soc. Jpn.* **1967**, *22*, 710–718.
(19) Curik, R.; Gianturco, F. A.; Lucchese, R. R.; Sanna, N. *J. Phys. B* **2001**, *34*, 59–79.
(20) Stoecklin, T.; Gianturco, F. A. *Eur. Phys. J. D* **2007**, *42*, 85–91.
(21) Stoecklin, T.; Gianturco, F. A. *Chem. Phys.* **2007**, *332*, 145–151.
(22) Stoecklin, T.; Gianturco, F. A. *Eur. Phys. J. D* **2006**, *40*, 369–375.
(23) Cederbaum, L. S.; Domcke, W. *J. Phys. B* **1981**, *14*, 4665–4689.
(24) Bardsley, J. N. *J. Phys. B* **1968**, *1*, 349–364.
(25) Orel, A. E.; Kulander, K. C. *Phys. Rev. Lett.* **1993**, *71*, 4315–4318.

(26) Taioli, S.; Tennyson, J. *J. Phys. B* **2006**, *39*, 4379–4392.
(27) Goumans, T. P. M.; Gianturco, F. A.; Sebastianelli, F.; Baccarelli, I.; Rivail, J. L. *J. Chem. Theory Comput.* **2009**, *5*, 217–221.
(28) Panosetti, C.; Baccarelli, I.; Sebastianelli, F.; Gianturco, F. A. *Eur. Phys. J. D* **2010**, *60*, 21–30.
(29) Bauschlicher, C. W., Jr.; Schaefer, H. F., III; Bagus, P. S. *J. Am. Chem. Soc.* **1977**, *99*, 7106–7110.
(30) Carter, E. A.; Goddard, W. A., III. *J. Chem. Phys.* **1988**, *88*, 1752–1763.
(31) Gutsev, G. L.; Ziegler, T. *J. Phys. Chem.* **1991**, *95*, 7220–7228.
(32) Russo, N.; Sicilia, E.; Toscano, M. *J. Chem. Phys.* **1992**, *97*, 5031–5036.
(33) Cai, Z.-L. *J. Phys. Chem.* **1993**, *97*, 8399–8402.
(34) Schwartz, M.; Marshall, P. *J. Phys. Chem. A* **1999**, *103*, 7900–7906.
(35) Sendt, K.; Bacskay, G. B. *J. Chem. Phys.* **2000**, *112*, 2227–2238.
(36) Chau, F. T.; Mok, D. K. W.; Lee, E. P. F.; Dyke, J. M. *ChemPhysChem* **2005**, *6*, 2037–2045.
(37) Czernek, J.; Živný, O. *Mol. Phys.* **2008**, *106*, 1761–1765.
(38) Margulès, L.; Demaison, J.; Boggs, J. E. *J. Phys. Chem. A* **1999**, *103*, 7632–7638.
(39) Charo, A.; De Lucia, F. C. *J. Mol. Spectrosc.* **1982**, *94*, 363–368.
(40) Kirchhoff, W. H.; Lide, D. R., Jr.; Powell, F. X. *J. Mol. Spectrosc.* **1973**, *47*, 491–498.
(41) Qian, H. B.; Davies, P. B. *J. Mol. Spectrosc.* **1995**, *169*, 201–210.
(42) Burkholder, J. B.; Howard, C. J.; Hamilton, P. A. *J. Mol. Spectrosc.* **1988**, *127*, 362–369.
(43) Murray, K. K.; Leopold, D. G.; Miller, T. M.; Lineberger, W. C. *J. Chem. Phys.* **1988**, *89*, 5442–5453.
(44) Schwartz, R. L.; Davico, G. E.; Ramond, T. M.; Lineberger, W. C. *J. Phys. Chem. A* **1999**, *103*, 8213–8221.
(45) Mathews, C. W. *J. Chem. Phys.* **1966**, *45*, 1068.
(46) Graupner, K.; Field, T. A.; Mayhew, C. A. *New J. Phys.* **2010**, *12*, 083035.